Ionic Liquid Chiral Resolution: Dissociation of Methyl 2-Ammonium Chloride Propanoate on Al(854)^S Surface

Nobar Jalili,[1] Narjes Ansari,[1] Francesc Viñes,[2] Francesc Illas,[2,*] and Fariba Nazari[1,3]

[1] *Faculty of Chemistry, Institute for Advanced Studies in Basic Sciences (IASBS), 45195-1159 Zanjan, Iran*

[2] *Departament de Química Física & Institut de Química Teòrica i Computacional (IQTCUB), Universitat de Barcelona, C/Martí i Franquès 1, 08028 Barcelona, Spain*

[3] *Center of Climate Change and Global Warming, Institute for Advanced Studies in Basic Siences, 45195-1159, Zanjan, Iran*

[*]corresponding author: francesc.illas@ub.edu

Abstract

The adsorption of the chiral methyl 2-ammonium chloride propanoate ionic liquid on the chiral Al(854)^S surface has been investigated by density functional calculations on periodic slab models. The results show that the molecule features an enantioselective dissociative adsorption at the surface chiral center. The low-coordination of Al atoms at kinked steps and the strong attractive forces towards molecular O atoms are the main causes of the dissociation. At the surface, 2-ammonium propanal, methoxy groups, and Cl atoms are generated, attached at different sites depending on the precursor enantiomer. The adsorption strengths reveal that the bonding of *R*-enantiomer is more favorable than *S*-enantiomer by 0.08 eV, enough for a chiral resolution process with an enantiomeric excess of ~96%, whereas adsorption on achiral Al(111) surface reveals no enantiomeric discrimination with a weak molecular adsorption and no dissociation. Enantiomeric discrimination on chiral Al(854)^S surface is possible due to different semicore molecular levels binding energies and to distinct infrared vibrational fingerprints. The present results open the possibility for a rather simple way to separate these enantiomers.

1. Introduction

Phenomena associated with chiral molecules —non-superimposable mirror images called enantiomers— have held a deep fascination for scientists since Pasteur's initial discovery of enantiopure sodium ammonium tartrate crystals in the 1850s.[1] At a deep level, the observation that biological life is essentially homochiral (observed amino acids and sugars are almost exclusively of the *L*- and *D*-forms, respectively) raises profound issues regarding the origin of life and continues to spur vigorous debate.[2]

The fact that different enantiomers of organic molecules can have radically different biological effects is also well documented. Enantiomeric forms of a medicines oftentimes show markedly different efficacy or even trigger completely different metabolic responses. For instance *R*-ibuprofen is over 100 times more potent than *S*-ibuprofen.[3] Thalidomide is one of the most tragic examples; *R*-thalidomide is a sedative whereas *S*-thalidomide is known to cause birth deformity.[4] Nevertheless the usage of enantiopure medicines has many advantages: From more-selective and less-complex pharmacokinetic profiles to improved therapeutic indexes. This settled the guideline issues of the Food and Drug Administration and of the European Medicines Agency favoring the development of new drugs with enantiospecific chirality,[5,6] which has led to an enormous market for single-enantiomer drugs.

Enantiopure molecules tends to be nowadays obtained *via* the synthesis of racemic mixtures containing equal parts of *R*- and *S*-forms, and the subsequent separation by chiral resolution, usually carried out by high-performance chromatographic techniques using pure chiral selector solid phases.[7] Alternatively there has been a notorious advance in the homogeneously-catalyzed asymmetric synthesis, such as the enantioselective hydrogenation,[8]

although steps are still needed to separate the enantiomeric compounds from media and catalyst, or even to improve the degree of purity, normally quantified by the enantiomeric excess (*ee*).

A particularly interesting physical process to differentiate and separate the two enantiomers of a chiral species is the enantiospecific adsorption on a solid surface which is itself chiral at the molecular length scale. Work on developing solid surfaces that are chiral has spread over the last decades, with a large body of research focused on creating enantioselective heterogeneous catalysts that combine catalytically active metals with enantiopure organic template molecules.[9] In this scheme, a template enantiopure chiral molecule is chosen so that irreversibly binds to the catalyst surface and bestows chirality to the resulting functionalized catalyst. This concept has been successfully applied to the enantioselective hydrogenation of α-ketoesters over tartaric acid tethered Ni catalysts,[10,11] and the hydrogenation of β-ketoesters over Pt catalysts template with cinchona alkaloids.[12-14]

A complementary alternative route is to develop surfaces that are intrinsically chiral, without the need of docking chiral molecules on them. This has been usually pursued on chiral surfaces cut from achiral solids, such as transition metals,[15-17] but also on naturally chiral compounds, like quartz, whose chirality stems from a enantiospecific helical arrangement of silica tetrahedra. For instance, asymmetric synthesis of chiral pyrimidyl alkanols was demonstrated in the experiments by Soai *et al*,[18] and chiral resolution of aminoacids has been recently tackled on quartz $(10\bar{1}0)$ surface.[19]

In this paper we explore the enantioselective chemisorption of *R*- and *S*-methyl 2-ammonium chloride propanoate ionic liquid on achiral Al(111) and on chiral Al(854)^S surfaces, given the potential versatility of using ionic liquid forms of drugs instead of organic salts.[20] To the best of our knowledge this is the first *ab initio* study on chiral resolution of an ionic liquid

using a chiral stepped metal surface. Our Density Functional (*DF*) theory based calculations on periodic slab models aid in the understanding of enantiospecific surface adsorption by providing detailed information of adsorption geometries, electronic structure, vibrational fingerprints, and bonding energies.

2. Computational Details

We performed periodic slab model calculations based on DF theory with the VASP code[21] using the Perdew-Burke-Erzenhof (*PBE*) exchange correlation functional,[22] given that it provides a rather balanced description of metals.[23] The projector augmented wave method has been used to represent the atomic cores.[24] At first, Aluminum bulk optimization was carried out using a plane wave expansion cutoff energy of 475 eV. A 10×10×10 Monkhorst-Pack[25] grid of special **k**-points was used to carry out the numerical integration on the reciprocal space. This optimized Al cell parameter of 4.02 Å was used for the subsequent simulation of the surface. Briefly, the chosen Al(854)^{S} chiral surface was modeled by a (2×2) surface unit cell with a minimum vacuum spacing of 10 Å. Initial adsorption site sampling was carried out with a 3.35 Å slab width, and a 4×3×1 Monkhorst-Pack **k**-points grid. Here a reduced plane wave kinetic energy cutoff of 350 eV was used, and, in addition, only the adsorbate atoms were allowed to relax, i.e. the Al surface was kept fixed, since no difference was observed in the molecule location when the surface layers were relaxed. In successive steps, the most stable configurations were refined at **Γ** point but with a 10.1 Å slab width and with a 475 eV cutoff. In this set of calculations, the three outermost Al layers were allowed to relax, yet the bottomost Al layer was kept frozen at bulk-optimized positions to provide an adequate bulk environment to the surface. Geometric relaxations were performed using a quasi-Newton algorithm[26] until forces on each unconstrained atom were less than 0.01 eV Å^{-1}. For the ionic liquid molecule both enantiomers were optimized

at the **Γ** point placing the isolated molecule inside the studied surface unit cell but without the metal surface, and in all cases avoiding interaction between translationally created replicas. For the molecule adsorption investigation on Al(111) surface a (6×3) supercell was employed, with a 475 eV cutoff energy and a 3×4×1 **k**-points grid.

In order to determine the most stable molecular arrangement for the ionic liquid molecule adsorbed on Al(111) and Al(854)^S surfaces, structural optimizations have been performed starting from more than 60 initial trial geometries, differing both in location and orientation above the two surfaces unit cells. In particular, top, bridge, and hollow sites involving the atoms exposed by the surface have been considered, but also different tilting angles and orientations of the incoming ionic liquid molecule. The molecular adsorption energy, E_{ads}, of the different structures has been computed as usual following:

$$E_{ads} = (E_s + E_{il}) - E_{s/il} \qquad (1)$$

where $E_{s/il}$ is the energy of either the Al(111) or the Al(854)^s surface with the adsorbed ionic liquid, E_{il} is the energy of the ionic liquid molecule in vacuum, and E_s is the energy of the bare Al(111) or Al(854)^s slabs. Within this definition the more positive the E_{ads} values the stronger the adsorption. All optimized structures were further characterized as local minima in the potential energy surface by a proper vibrational frequency analysis, carried out by the numerical calculation and diagonalization of the Hessian matrix, constructed from finite differences of analytical gradients. The elements of the Hessian matrix have been obtained by calculating energy changes due to independent displacements of 0.03 Å of every molecular atom in each direction of the unit cell vectors.

Simulated infrared (IR) spectra have been obtained estimating the intensity of a band through the change of the dipole moment component normal to surface accompanying a given vibration. The spectra have been drawn by smoothing the peaks with a Gaussian function of 100 cm^{-1} half width. This procedure has been widely used in the past for calculations of adsorbate

spectra on solid metal surfaces.[27,28] Note that due to the dipole parallel component cancellation by the specular counterdipole created by the metal surface electron density cloud, only vibrations with a dipole component normal to the surface are detected.

3. Surface Chirality Notation

Here we briefly review some useful notation for describing chiral single-crystal surfaces of simple metals since this information is not so widely known. We focus on pure metals with face-centered cubic (*fcc*) crystal structure, but the origins of surface chirality applied on these materials are extendable in a very straightforward way to other crystal structures with more higher complexity, such as alloys and metal oxides. Indeed a great variety of materials exist as enantiomorphic solid; the best known examples are molecular crystals of single organic molecule enantiomers. Many inorganic compounds have also enantiomorphic crystal structures, such as the above-commented quartz. Note that these materials are intrinsically chiral due to the lack of symmetry in their bulk unit cell or the basis defining the atomic positions within the cell.

For the present purposes, it is important to realize that even highly-symmetric materials can be tailored to render crystal faces that are chiral. For example, let us consider the (854) and ($\overline{8}\overline{5}\overline{4}$) surfaces of *fcc* Al, pictured in Figure 1a. Each surface can be regarded as atomically-flat (111) terraces separated by one-atom-in-height steps. Note that step edges are not straight, but they rather consist of periodic repetitions of straight three-atom-in-length step edges separated by a kink atom. This crucial point is what makes both surfaces non-superimposable mirror images, and, therefore, chiral.

For the notation of chiral surfaces, McFadden *et al*. proposed a set of rules[29] similar to the Cahn-Ingold-Prelog (*CIP*) notation for organic molecules.[30] Briefly, within this notation one views the surface from above and draws a circle directed from the long edge to the short edge of the step, and finally to the lower terrace. Surface is denoted *R* (*S*) when the circle is oriented

clockwise (counterclockwise), see Figure 1a. In this work it was shown that all pure metal surfaces with asymmetric steps —i.e. steps with straight segments of unequal length— are chiral.[29] However, Ahmadi and coworkers pointed out that this definition does not include all possible chiral surfaces, since only segments lengths are considered, and not their particular nature.[31] This fact is clearly illustrated by the Al(531) in Figure 1b, whose kinked steps have step segments with equal length, although the surface is in fact chiral; this is because step segments locally alternate (100) and (110) orientations —oftentimes referred as A and B steps, respectively. Enantioselective adsorption of serine amino acid on chiral Cu(531) surface has been recently reported,[32] and a similar situation was found on Pt(643) surfaces, which were experimentally found to feature an enantiospecific electro-oxidation of glucose.[31,33] In this sense the Ahmadi notation is more general and encompasses that of McFadden. Therefore, chiral surfaces can be named after the following procedure: The surface is viewed from above and the {111}, {110}, and {100} facets that intersect to form the kink in the surface —the distinction between {*hkl*} and (*hkl*) surfaces will be made clear below. Similarly to McFadden, a circle is drawn directed from the most to the least densely-packed surface facets, i.e. {111}→{100}→{110}, being the surface *R* (*S*) when the circle is oriented clockwise (counterclockwise). On the following we adopted the more general Ahmadi notation.

Note that facet ordering is dependent on the bulk crystal structure packing. In this sense, it would be different, for example, for body-centered cubic (*bcc*) crystals. Focusing on *fcc* (*hkl*) surfaces, it is obviously interesting to know whether a given surface is chiral for an arbitrary set of Miller indices, and whether *R* or *S* chirality can be succinctly described. Next, we describe how each of these issues can be resolved in a simple way. To this end we consider the van Hove and Somorjai usual Miller indices notation,[34] where;

$$(hkl) = l(111) + (k\text{-}l)\{110\} + (h\text{-}k)\{100\} \quad (2)$$

and h, k, and l are the surface Miller indices. To identify the low Miller index surfaces the first vector is fixed to be (111), and the {110} notation is to encompass (101), (110), and (011) facets, whereas similarly {100} encompasses (010), (100), and (001) facets. Thus, without loss of generality, we assume that $h \geq 0$, $k \geq 0$, and $l \geq 0$. Note that surfaces of *fcc* metals with two negative Miller indices are structurally identical to the surface with all positive indices. Surfaces with one or three negative Miller indices are the mirror image of the surface with positive indices, whenever this surface is chiral.

The assignment of the appropriate low Miller index directions in Eq. 2 can be made with the aid of Figure 2a, which shows the {110} and {100} vectors as viewed looking along the (111) vector towards the origin. These vectors divide the diagram into six regions, each corresponding to a particular class of (*hkl*) Miller indices. To use the diagram, we first locate the section of interest. In our case the *fcc* Al(854) surface has $h > k > l$, and, consequently this surface should be decomposed as:

$$\text{Al}(854) = 4\cdot\text{Al}(111) + 1\cdot\text{Al}(110) + 3\cdot\text{Al}(100) \quad (3).$$

The usefulness of Eq. 2 is immediately apparent: For a *fcc* surface to be chiral it must have kinked steps made by the intersection of three different low Miller index surfaces. Thus, any (*hkl*) surface with non-zero indices —$h \neq 0$, $k \neq 0$, $l \neq 0$— and no equal indices —$h \neq k \neq l$— is chiral. Figure 2b can be used to assign the *R* or *S* designation to a k (*hkl*) surface following the notation of Ahmadi et al,[31] by stating *R* (*S*) chirality to clockwise (counterclockwise) directions. Note that the diagram considers only positive indices, but equivalency to negative indices is straightforward. Furthermore, Figure 2b shows that when switching two of the indices the new surface is also enantiomorphic. Consequently, there are 48 chiral *fcc* (*hkl*) surfaces obtained by

±*h*, ±*k*, and ±*l* permutations, which can be separated into two classes involving 24 surfaces each. For each class all permutation surfaces are equivalent, and enantiomorphic to the others in the opposite class.

4. Adsorption of Methyl 2-Ammonium Chloride Propanoate on Al(111) and Al(854)^{S} Surfaces

Let us start with the adsorption of *R*- and *S*-methyl 2-ammonium chloride propanoate ionic liquid molecules on the achiral Al(111) surface. Aluminum is the selected metal because features a *fcc* crystal structure, similar to other transition metals used for enantiospecific adsorption such as the above-commented Cu and Pt, plus it is economically affordable. The Cl is the counterion of the cation part of the ionic liquid, which consists of a derivative of Alanine but with its carboxylic group converted into an ester. As described in the Computational Details, a (6×3) unit cell is used, in which the bottommost Al layer is kept in bulk-optimized positions, whereas the two uppermost Al layers are fully optimized together with the molecule. Different molecular configurations were examined on various active sites of the surface, yet only the most stable configurations of *R*- and *S*-enantiomers are shown in Figure 3. Clearly, and as expected from the surface achirality, both enantiomers interact with Al(111) surface in a very similar manner and, in both cases, there is a molecular adsorption. For any of the two enantiomers, the Cl atom sits on top of a surface Al atom, at a distance of ~2.35 Å. Note that such interaction pulls the attaching surface Al atom towards the vacuum. On the cationic part, the N-H bond lengths of the amino groups are ~1.06 Å, and the molecule closest distance to Al(111) surface plane is approximately 2.5 Å. This is a clear indication of a physisorption state, and correlates with the estimated adsorption energy of 0.83 eV. A figure which will become larger if explicitly including dispersion forces not accounted for in the PBE functional but affecting equally the two

enantiomers. Overall, we can claim that on the Al(111) surface, the ionic liquid features a non-enantioselective physisorption.

Let us now investigate the effect of low-coordinated sites at steps of Al(854)^{S} chiral surface on the enantiospecific adsorption of *R*- and *S*-methyl 2-ammonium chloride propanoate. As commented in the Computational Details, more than 60 conformations were explicitly relaxed for each enantiomer in the geometry optimization procedure, considering different top, bridge, and hollow sites of the Al surface, as well as distinguishing among kink, corner, step, and terrace sites; all in all a challenging aspect in order to find the global adsorption minimum, although chemical guidance was taken from previous studies addressing the interactions of O, Cl, and N atoms with Aluminum.[35-37] Only a few suitable adsorption conformations were later on refined, yet solely the most favored adsorptive configurations for both *R* and *S* enantiomers are shown in Figure 4, given that other arrangements were at least 0.2 eV less stable, and, therefore, not suitable to be sampled during the adsorption process. One of the first distinct features compared to achiral Al(111) surface is the dissociative molecular adsorption. In both cases not only the Cl anion is separated from the Alanine derivative, but also a methoxy group is separated from the ester group, directly attaching to the Al surface. Dissociative adsorption on Aluminum surfaces has been observed for other molecules.[38,39]

Focusing on the *R*-enantiomer, the Cl atom is 2.25 Å distant from Al kink atom, the Oxygen atom from the methoxy group is bridging step and kink Al atoms with bond lengths of 1.86 and 1.98 Å, respectively, while the dehydrogenated *R*-2-amino propanal species —hereafter named *R*-Ala— is interacting with terrace Al atoms through its carboxyl group, with Carbon-Aluminum distances of 2.04 and 2.16 Å. In the case of *S*-enantiomer, the Cl atom lies on top of a terrace Al atom with a bond length of 2.30 Å, the dissociated methoxy group features a strong

interaction between its O atom and the kink Al atom, situated at 1.93 Å, and finally, the *S*-Ala is again adsorbing through its carboxyl group but now with its Carbon atom bridging kink and terrace Al atoms, with bond lengths of 2.00 and 2.15 Å. In both chiral molecules the amino groups are kept essentially intact, with N-H distances of 1.03-1.05 Å.

The estimated adsorption energies are 2.91 and 2.83 eV for *R*- and *S*-enantiomers, respectively. This implies a difference in adsorption energy of 0.08 eV —7.9 kJ mol^{-1}—, in the range of other reported energy differences on enantioselective adsorption processes.[40-42] Assuming a steady-state surface situation at 300 K, a Maxwell-Boltzmann distribution implies a ~96% *ee* of *R*-enantiomer. In a very straightforward way, and because of the specular symmetry, the same *ee* is expected for *S*-enantiomer on the $Al(\bar{8}\bar{5}\bar{4})^R$ surface. The other important characteristic is the amazingly increased adsorption energy of both enantiomers, which are roughly three times larger than the adsorption energy on the Al(111) surface. This is due to the higher ratio of low-coordinated sites, and their enhanced surface activity and flexibility to accommodate surface species, as already found for other *fcc* metals.[28,43] This adds up for the utilization of other surfaces with a higher *l* Miller index, since the adsorption of the ionic liquid is strongly thermodynamically driven to the chiral steps, and on (111) terraces one would observe only racemic mixtures of both enantiomers.

To obtain a better picture of the enantioselective dissociative adsorption, we calculated the charges associated to each atom according to a Bader analysis,[44,45] It is found that both *R*- and *S*-enantiomers withdraw charge from the $Al(854)^S$ surface when adsorbed; in particular, 4.84 and 4.47 electrons, respectively. This may appear as a too large charge transfer but one must warn about the difficulty to define atomic charges in a metal where the electrons are largely delocalized, and present Bader charges analysis must be considered as exploratory. To this end, a

plot of Bader charges difference with respect the isolated molecule and pristine surface is shown in Figure 5. This reveals that the transferred charge is essentially accumulated in the C atom of the aldehyde group of Ala species. This is due to two main factors: First, the C atoms changes from an ester situation with two electrophile O atoms to the aldehyde situation with only one O. Secondly, part of the charge transfer is accumulated on this C, since it is the closest one to the Aluminum surface. The large negative charge provokes a reorganization of the electron density in the surrounding area, observable in a few subtle effects. For instance, surface Al atoms rearrange their charges in a complex fashion —with some surface Al atoms gaining electron density— but overall with surface Al atoms beneath the Ala moiety featuring a positive charge, in order to compensate the negative charge on the C carbon. Furthermore, the Cl anion, which was counteracting the positive organic cation of the ionic liquid, loses charge, given the reduced positive charge of the Ala group.

A deeper analysis has been carried out by projecting the Density of States (*DOS*) of both enantiomers, as shown in Figure 6. The DOS of the $Al(854)^S$ surface when attaching *R*- or *S*-enantiomers remains essentially the same as in the naked surface situation, with almost no distinguishable effect of the surface→molecule charge transfer, and Al 3*s* and 3*p* states spanning energies from ~-11 eV to Fermi level (E_F). More insight is gained looking at the chiral molecule orbitals. Due to the molecular level realignment, the Chlorine *3p* and 3*s* atomic levels are shifted to lower binding energies by ~3.5 eV compared to the isolated molecule, although the atomic character is preserved on both, with no mixing with Al surface states, i.e. revealing a strong ionic character of the Cl atom. Concerning 3*p* orbitals, they are found at the same energy for both enantiomers, but coinciding in energy with the Al band. In the case of the 3*s* states, the one from the *R*-enantiomer is shifted ~0.3 eV towards lower binding energies compared to the *S*-

enantiomer, enabling its differentiation. Regretfully, Ala methyl group related orbitals are appearing at the same range of energies, and because of this a clear observation would be impossible. As far as Ala and methoxy species are concerned, most molecular orbitals are located in the Aluminum *sp*-band region, and, for some of them, a significant hybridization with Al surface states is observed, highlighting the above-commented strong interaction between the generated moieties and the Al(854)^{S} surface. Below the Aluminum band edge energy one finds molecular orbitals with no overlap. In particular, ammonia bands are found near the band edge energy, with a strong N-H covalent character. Note that the lower band of *R*-enantiomer is downshifted by ~0.35 eV compared to the *S*-one, and in this sense this molecular orbital could be used in the enantiomer identification. Furthermore, the semicore O 2*s* level of the Ala species is upshifted by ~0.7 eV compared to the *R*-enantiomer, which can be served as well for the *in situ* discrimination of the enantiomeric species by means of photoemission spectroscopies.

In order to investigate whether spectroscopic differentiation of the two enantiomers is achievable with a less invasive technique, the vibrational IR fingerprints of both adsorbed enantiomers have been calculated and simulated spectra plotted in Figure 6. In general terms both molecules have coincident spectra, with clear features in two particular regions, the 900-1400 cm^{-1} zone, and the one spanning 3000-3400 wavenumbers. In the later, for instance, one detects a peak at ~3415 cm^{-1} which belongs to a N-H bond stretching of the amino group, in particular that oriented towards the vacuum. The difference of 5 cm^{-1} between the *R*- and *S*-spectra would make it rather cumbersome to differentiate among both species. The N-H stretching oriented towards the Aluminum surface does present a peak at 3000 cm^{-1} for both enantiomers, although here a much more intense signal is envisioned for the *R*-enantiomer, which goes along with the above-commented larger charge transfer, and, consequently, a larger

dipole moment. Therefore, the appearance of a high intense band at 3000 cm^{-1} can be taken as indicative of the majority presence of adsorbed *R*-enantiomer molecules which indeed exhibit stronger interaction with the surface.

One finds more interesting features at the lower frequency region, as seen in Figure 6. Above 1000 cm^{-1} many Ala torsion and bending modes are found, which are indeed different for both enantiomers, note for instance the umbrella mode of *R*-Ala centered at 1180 cm^{-1}, blue-shifted by 25 cm^{-1} with respect the *S*-enantiomer. However the zone is crowded, and it would be probably difficult to unequivocally ascertain particular peaks; a more likely outcome is a broad band with many contributions. Another peculiarity of the system is the absence of the C=O aldehyde stretching signals from Ala, due to parallel disposition of such group with respect the metal surface, which makes its stretching invisible to IR techniques.

Last but not least, the most suitable form to distinguish both enantiomers by means of vibrational spectroscopies is, curiously, by detecting the achiral methoxy moiety created during the dissociative adsorption. In fact, in both cases the methoxy C=O vibration is visible, since the moiety adsorbs rather perpendicular to the surface, and comes to be located in a rather clear area of the IR spectrum, below 1000 cm^{-1}. The stretching is located at 963 cm^{-1} for the *R*-enantiomer adsorption, whereas the one generated from the adsorption of *S*-enantiomer is blue-shifted by 33 cm^{-1}, and thus located at 996 cm^{-1}. Such difference is *a priori* enough to distinguish both cases in standard vibrational spectroscopies, and consequently, it is introduced as a non-aggressive and simple method to differentiate among both enantiomers.

5. Conclusions

Here we examined the enantiospecific chemisorption of *R*- and *S*-methyl 2-ammonium chloride propanoate ionic liquid on achiral Al(111) and on chiral $Al(854)^S$ surfaces. This has

been tackled *via* a thorough sampling of adsorption sites and conformations for both enantiomers on both surfaces, carrying out DF optimizations on periodic slab models. Both enantiomers are found to molecularly adsorb very similarly on the achiral Al(111) surface, with an estimated adsorption energy of 0.83 eV, thus revealing, as expected, a non-enantiospecific adsorption of the ionic liquid on an achiral Aluminum surface.

When it comes to the chiral Al(854)^{S} surface —and those related by specular and/or crystallographic symmetry— the ionic molecule undergoes, for both enantiomers, an spontaneous dissociative adsorption, mediated by the strong interaction with the low-coordinated Al atoms located at chiral sites of the surface kinks. The dissociation not only implies the separation of the Chlorine anion, but also the breaking of the ester group of the cation, thus creating a dehydrogenated 2-ammonium propanal moiety attached to the Aluminum surface *via* its carboxyl group, and a methoxy species adsorbing *via* its Oxygen atom. Indeed the dissociative adsorption is *a priori* enantioselective, in the sense that the bonding of *R*-enantiomer is more favorable than *S*-enantiomer by 0.08 eV, enough for a chiral resolution process with an enantiomeric excess of 96%, assuming a steady-state Maxwell-Boltzmann distribution.

The enantioselective dissociative adsorption implies a charge transfer from the Al(854)^{S} surface to the ionic liquid molecule, concentrated around the aldehyde Carbon center, according to a Bader electron density analysis. This charge transfer induces an electron density reorganization on the generated surface moieties and the formation of a surface dipole moment perpendicular to the surface. The structural, energetic, and electronic changes are reflected in the projected DOS, with shifts of molecular orbitals located in the semicore energy that could allow for the enantiomer differentiation by means of photoemission spectroscopies, such as the O 2*s* level of the dehydrogenated aldehyde. A mostly harmless characterization by IR techniques

seems feasible according to simulated vibrational infrared fingerprints, which reveal a different location of the methoxy C=O stretching vibration centered at 963 and 996 cm^{-1} for *R*- and *S*-enantiomer adsorptions, respectively.

To summarize, the chiral surface of a simple, abundant, and inexpensive metal is found to be able to differentiate the two enantiomeric forms of a chiral ionic liquid, which opens the possibility for a rather simple way to separate these enantiomers —and probably others— for instance by an appropriate series setup of wetting (adsorption) and desorption cycles.

Acknowledgements

F. N. is grateful to the Institute for Advanced Studies in Basic Sciences, for financial support. This work was supported by the Spanish MICINN (grants FIS2008-02238 and CTQ2012-30751, CTQ-2010-14872/BQU) and, in part, by the Generalitat de Catalunya (grants 2009SGR1041 and XRQTC). F.V. thanks the MINECO for a postdoctoral *Juan de la Cierva* grant (JCI-2010-06372) and F.I acknowledges additional funding through the 2009 ICREA Academia award.

Figure 1. a) Ball models of (854) —left— and ($\bar{8}\bar{5}\bar{4}$) —right—of *fcc* Al surfaces with step edges highlighted in yellow. Terrace atoms are highlighted in pale-pink color. Red, blue, and brown squares represent {110}, {100}, and {111} facets, respectively. The dotted line represents a mirror plane. b) Ball model of (531) *fcc* surface

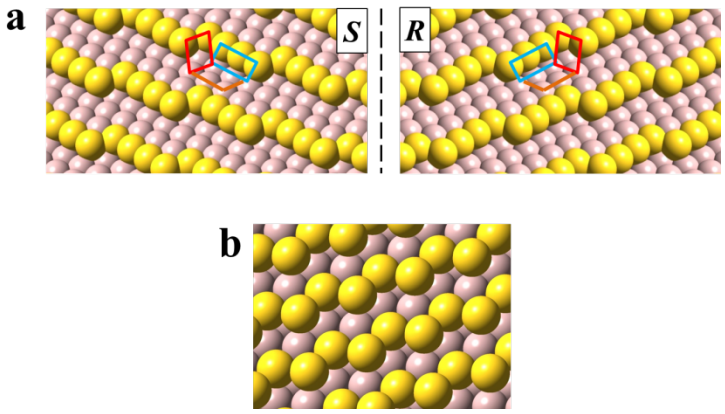

Figure 2. a) Graphical method for assigning microfacets decomposed as *fcc* (*hkl*) surfaces. b) Graphical construction for assigning *R* and *S* notations to *fcc* (*hkl*) surfaces. Note that both diagrams are for surfaces where all three indices are positive.

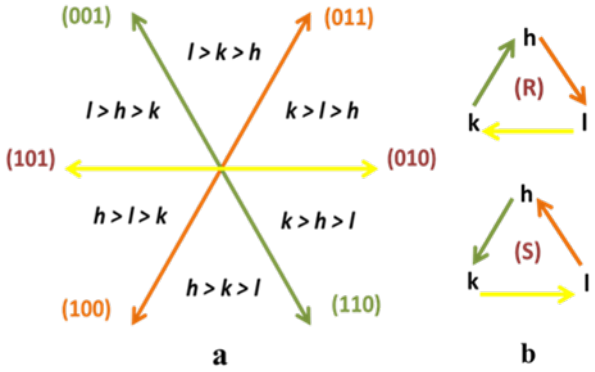

Figure 3. Most stable adsorption configurations of *R*- and *S*-methyl 2-ammonium chloride propanoate on the achiral Al(111) surface. Green, red, blue, grey, and white spheres denote Cl, O, N, C, and H atoms, respectively.

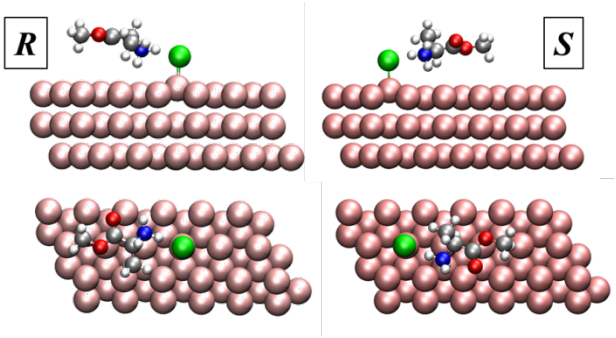

Figure 4. Most stable adsorption configurations of *R*- and *S*-methyl 2-ammonium chloride propanoate on the chiral Al(854)^{S} surface.

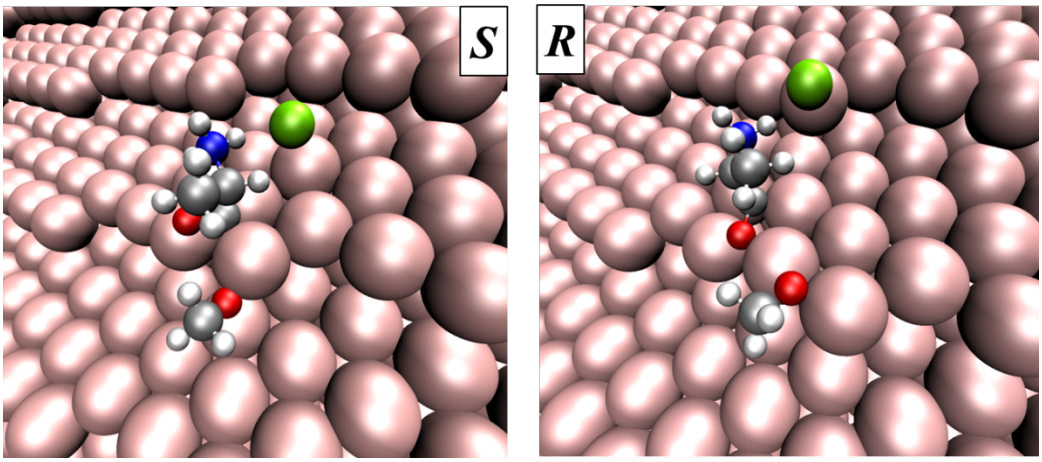

Figure 5. Bader charge differences for *R*- and *S*-enantiomers adsorbed on Al(854)^{S} chiral surface compared to a situation with no interaction between the molecule and the surface. The notation *CO, Ala,* and *MeO* designate whether the atom is within the aldehyde group of Ala, the Ala group, or the generated methoxy groups, respectively, or if they are Al atoms interacting with these groups.

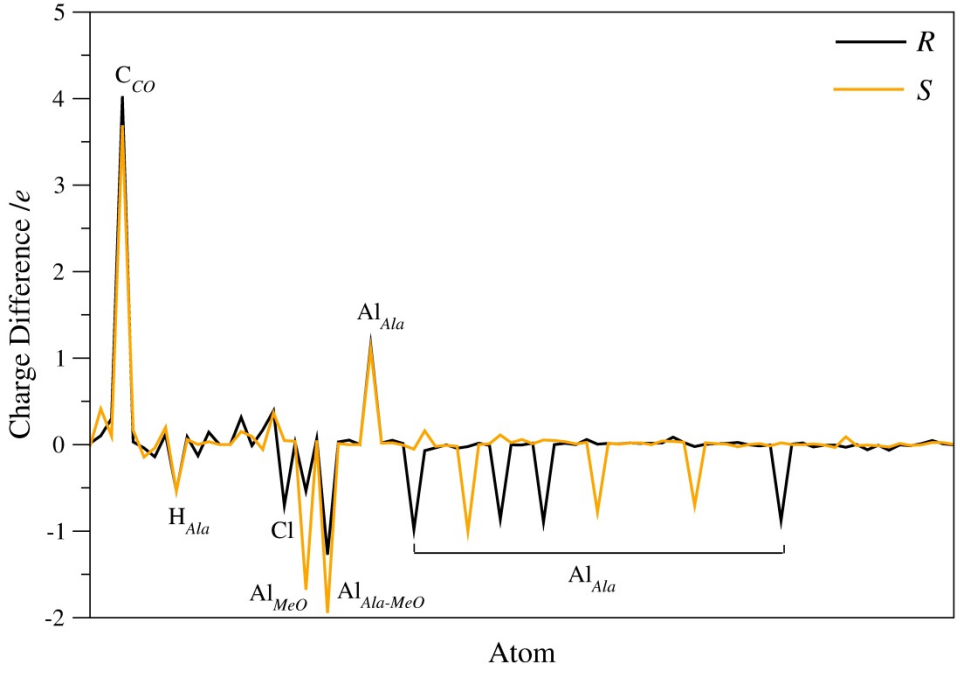

Figure 6. Projected DOS of the Al(854)^{S} surface decomposed into orbital contributions (top), as well as atomic decomposition for *R*- (middle) and *S*-enantiomers (bottom) adsorbed on it. Notations near peaks denote the orbital character, the surface moiety (Ala or MeO), and/or the radical contribution (methyl, CH_3, or ammonium, NH_3).

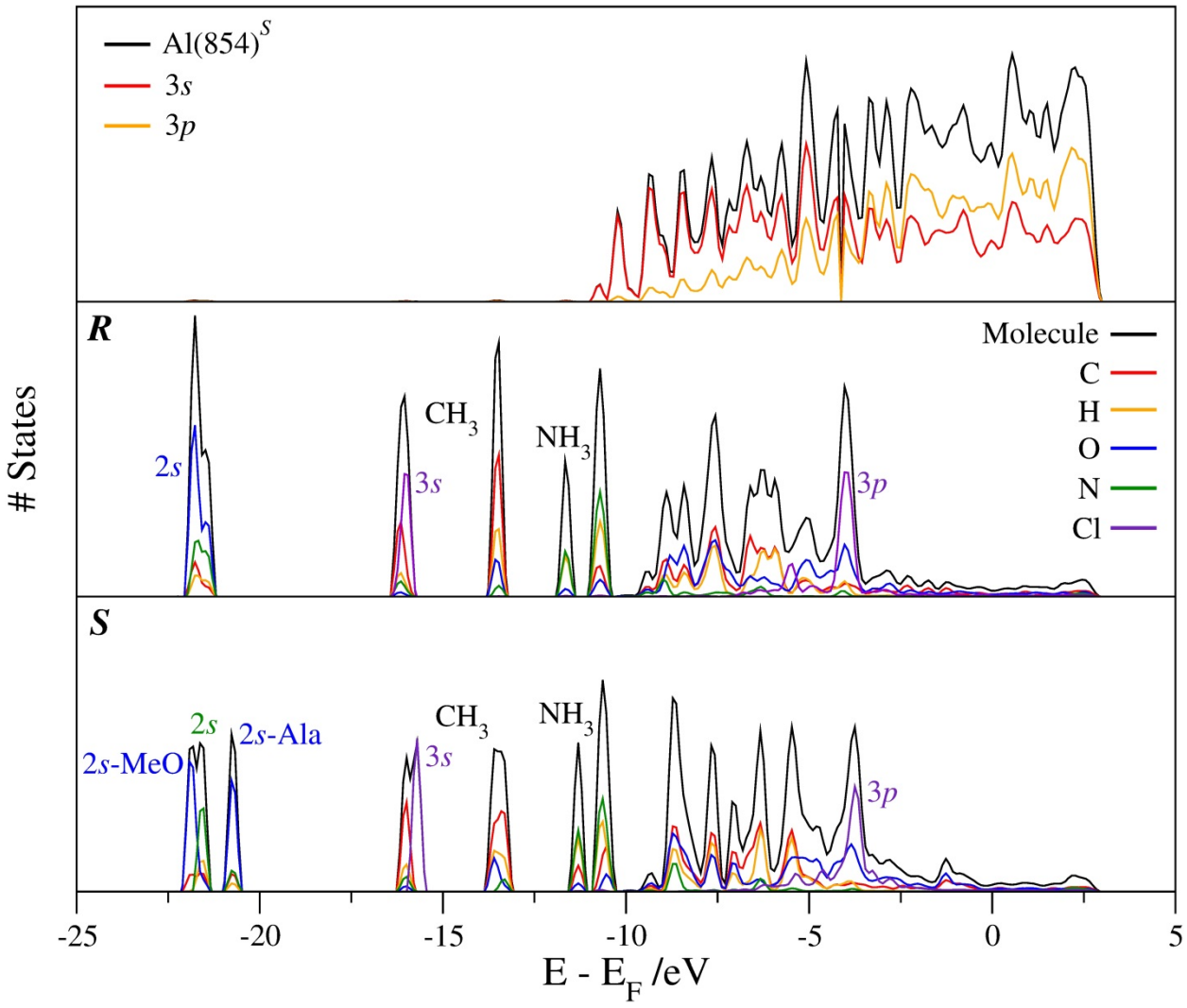

Figure 7. Simulated IR vibrational fingerprints of *R*- and *S*-enantiomers adsorbed on Al(854)^{S} chiral surface. Numbers near peaks denote the vibrational frequency in cm^{-1}. Sketches nearby depict the displacements of the vibrational shown with red arrows as a visual guide.

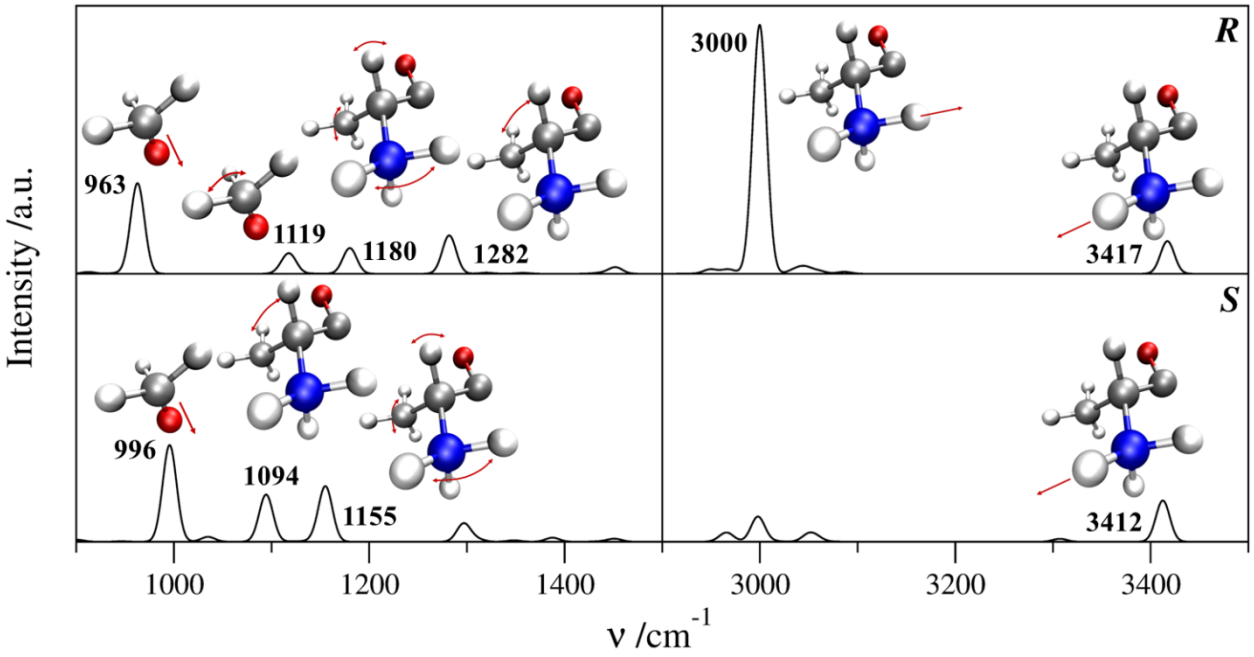

References

(1) Pasteur, L. *C. R. Acad. Sci. Paris* **1848**, *26*, 535-538.

(2) Bailey, J.; Chrysostomou, A.; Hough, J. H.; Gledhill, T. M.; McCall, A.; Clark, S.; Ménard, F.; Tamura, M. *Science* **1998**, *281*, 672-674.

(3) Tsai, S. W.; Lin, J. J.; Chang, C. S.; Chen, J. P. *Biotechnol. Prog.* **1997**, *13*, 82-88.

(4) Y. Takeuchi; T. Shiragami; K. Kimura; E. Suzuki; and N. Shibata, *Org. Lett.* 1999, **1**, 1571-1573.

(5) U. S. Food Drug Administration *Chirality* **1992**, *4*, 338-340.

(6) S. Branch in "*International Regulation of Chiral Drugs in Chiral Separation Techniques. A Practical Approach*", 2nd Edition, Weinheim, Wiley-VCH, 2001, 319-342.

(7) Izake, E. L. *J. Pharm. Sci.* **2007**, *96*, 1659-1676.

(8) a) Noyori, R. *Angew. Chem. Int. Ed.* **2002**, *41*, 2008-2022; b) Knowles, W. S. *Angew. Chem. Int. Ed.* **2002**, *41*, 1998-2007; c) Sharpless, K. B. *Angew. Chem. Int. Ed.* **2002**, *41*, 2024-2032.

(9) Jannes, G.; Dubois, V. *Chiral Reactions in Heterogeneous Catalysis*; Plenum Press, New York, 1995.

(10) Izumi, Y. *Adv. Catal.* **1983**, *32*, 215-271.

(11) Keane, M. A. *Langmuir* **1997**, *13*, 41-50.

(12) Garland, M.; Blaser, H. U. *J. Am. Chem. Soc.* **1990**, *112*, 7048-7050.

(13) Blaser, H. U.; Garland, M.; Jallet, H. P. *J. Catal.* **1993**, *144*, 569-578.

(14) Borszeky, K.; Mallat, T.; Baiker, A. *Catal. Lett.* **1996**, *41*, 199-202.

(15) Rankin, R. B.; Sholl, D. S. *Langmuir* **2006**, *22*, 8096-8103.

(16) Bhatia, B.; Sholl, D. S. *Angew. Chem. Int. Ed.* **2005**, *44*, 7761-7764.

(17) Greber, T.; Šljivancanin, Ž.; Schillinger, R.; Wider, J.; Hammer B. *Phys. Rev. Lett.* **2006**, *96*, 056103.

(18) Soai, K.; Osanai, S.; Kadowaki, K.; Yonekubo, S.; Sato, I. *J. Am. Chem. Soc.* **1999**, *121*, 11235-11236.

(19) Han, J. W.; Sholl, D. S. *Phys. Chem. Chem. Phys.* **2010**, *12*, 8024-8032.

(20) Stoimenovski, J.; MacFarlane, D. R.; Bica, K.; Rogers, R. D. *Pharm. Res.* **2010**, *27*, 521-526.

(21) Kresse, G.; Furthmüller, J. *Phys. Rev. B* **1996**, *54*, 11169-11186.

(22) Perdew, J. P.; Burke, K.; Ernzerhof, M. *Phys. Rev. Lett.* **1996**, *77*, 3865-3868.

(23) Janthon, P.; Kozlov, S. M.; Viñes, F.; Limtrakul, J.; Illas, F. *J. Chem. Theo. Comput.* **2013**, *9*, 1631-1640.

(24) Blöchl, P. E., *Phys. Rev. B* **1994**, *50*, 17953-17979.

(25) Monkhorst, H. J.; Pack, J. D. *Phys. Rev. B* **1976**, *13*, 5188-5192.

(26) Pulay, P. *Chem. Phys. Lett.* **1980**, *73*, 393-398.

(27) Happel, M.; Luckas, N.; Viñes, F.; Sobota, M.; Laurin, M.; Görling, A.; Libuda, J. *J. Phys. Chem. C* **2011**, *115*, 479-491.

(28) Luckas, N.; Viñes, F.; Happel, M.; Desikusumastuti, A.; Libuda, J.; Görling, A. *J. Phys. Chem. C* **2010**, *114*, 13813-13824.

(29) McFadden, C. F.; Cremer, P. S.; Gellman, A. J. *Langmuir* **1996**, *12*, 2483-2487.

(30) Cahn, R. S.; Ingold, C. K.; Prelog, V. *Experientia* **1956**, *12*, 81-94.

(31) Ahmadi, A.; Attard, G.; Feliu, J.; Rodes, A. *Langmuir* **1999**, *15*, 2420-2424.

(32) Eralp, T.; Ievins, A.; Shavorskiy, A.; Jenkins, S. J.; Held, G. *J. Am. Chem. Soc.* **2012**, *134*, 9615-9621.

(33) Attard, G.; Ahmadi, A.; Feliu, J.; Rodes, A.; Herrero, E. *J. Phys. Chem. B* **1999**, *103*, 1381-1385.

(34) van Hove, M. A.; Somorjai, G. A. *Surf. Sci.* **1980**, *92*, 489-518.

(35) Khan, G. G.; Bandyopadhyay, N. R.; Basumallick, A. *J. Phys. Chem. Solids* **2009**, *70*, 298-302.

(36) Kulkarni, B. S.; Krishnamurty, S.; Pal, S. *J. Phys. Chem. C* **2011**, *115*, 14615-14623.

(37) Pettus, K. A.; Taylorb, P. R.; Kummel, A. C. *Faraday Discuss.* **2000**, *117*, 321-329.

(38) Umezawa, N.; Kalia, R. K.; Nakano, A.; Vashista, P. *J. Chem. Phys.* **2007**, *126*, 234702.

(39) Borisov, A. G.; Teillet-Billy, D.; Gauyacq, J. P.; Silva, J. A. M. C.; Mertens, A.; Auth, C.; Winter, H. *Phys. Rev. B* **1999**, *59*, 8218-8231.

(40) Gellman, A. J.; Horvath, J. D.; Buelow, M. T. *J. Mol. Catal. A: Chem.* **2001**, *167*, 3-11.

(41) Bhatia, B.; Sholl, D. S. *Angew. Chem. Int. Ed.* **2005**, *44*, 7761-7764.

(42) Bhatia, B.; Sholl, D. S. *J. Chem. Phys.* **2008**, *128*, 144709.

(43) Viñes, F.; Lykhach, Y.; Staudt, T.; Lorenz, M. P. A.; Papp, C.; Steinrück, H.-P.; Libuda, J.; Neyman, K. M.; Görling, A. *Chem. Eur. J.* **2010**, *16*, 6530-6539.

(44) Bader, R. F. W. *Atoms in Molecules: A Quantum Theory*; Oxford Science, Oxford, U. K., 1990.

(45) Henkelman, G.; Arnaldsson, A.; Jonsson, H. *Comput. Mater. Sci.* **2006**, *36*, 354-360.

Table of Contents

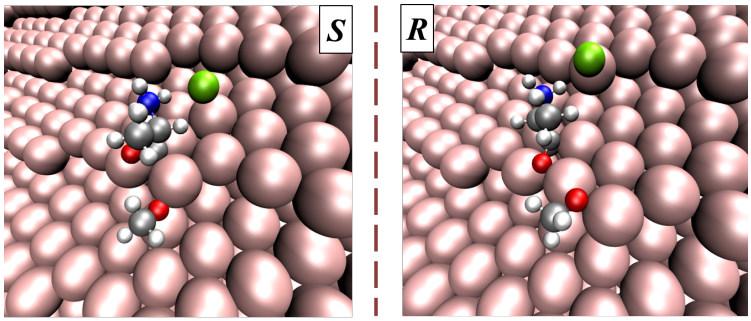

Ionic Liquid + Al(854)^{S} = Chiral Resolution